第 43 卷 第 12 期/2023 年 6 月/光学学报 研究论文

光学学报

海面空中目标的红外偏振辐射特性仿真分析

朱德燕[1,2*]，付晓萱[1,2]，唐骏伟[1,2]，刘晓磊[3]

[1]南京航空航天大学航天学院，江苏 南京 210001；

[2]南京航空航天大学空间光电探测与感知工业和信息化部重点实验室，江苏 南京 210001；

[3]中国空间技术研究院遥感卫星总体部，北京 100098

摘要 将偏振特性结合到强度信息中可有效提高天基系统对海面背景下空中目标的探测与识别性能，尤其是对于红外隐身目标。针对红外偏振特性、最优探测波段不明的问题，建立了基于天基平台的空中目标红外偏振辐射模型，分析了近红外到长波红外目标的偏振特性。采用偏振度作为评价指标，分析了目标辐射温度、飞行高度和天基探测俯仰角在红外波段中的偏振辐射规律。实验结果表明：对于不同飞行高度、辐射温度的目标而言，目标与海面背景的红外偏振特性在 9 μm 处差异显著，该波长可作为偏振探测的最佳波段；在最佳探测波段，相较于水平偏振而言，目标和背景的差异主要体现在垂直偏振分量上；当天基平台俯仰角为大角度掠地状态时，目标与背景的偏振度差值更大，有利于提高探测性能。

关键词 测量；偏振成像；红外特性；海面背景；天基探测；偏振度

中图分类号 O436.3；O439 **文献标志码** A **DOI**：10.3788/AOS222056

1 引 言

在目标与背景红外辐射强度对比度低的情况下，将偏振特性差异结合到强度探测中可显著提高系统的探测与识别能力[1-6]。随着红外多波段成像制导技术的不断发展[7-11]，如何利用偏振特性并合理选取探测波段以提高目标探测能力成为当前天基海面背景空中目标探测的一个热点与难点。

面向海面背景空中目标探测需求，Yuan 等[12-13]提出了基于遥感数据与物理模型耦合的海/云背景辐射特性一体化建模方法，探讨了飞机尾焰的成像特性，并进一步指出联合多个窄波段的探测性能可以优于宽波段。Ni 等[14-15]在全链路成像特征建模的基础上，进一步提出了通过空中目标信噪比和等效辐射强度等指标评价系统性能，从而优化波段选择。结合偏振与红外探测等光学监测方法是解决传统监测手段在海雾、耀斑和复杂光照等复杂海况干扰下探测能力受限的新思路[16]。面向可见光和近红外波段，针对传统光强手段难以有效识别和检测杂乱背景中的伪装目标的问题，王启超等[17]在 400～1000 nm 波段内对林地型背景中的铁板和迷彩伪装板进行了多光谱偏振探测实验，验证了偏振探测的有效性。针对中波和长波红外波段空中目标在复杂背景下的探测需求，王霄等[18]计算并分析了尾焰和蒙皮的红外辐射特性，发现长波偏振探测有利于增强目标成像的细节。针对中红外波段海面太阳耀光背景下传感器受到强干扰而无法有效探测的问题，李岩松等[19]利用偏振手段有效削弱了不同场景下的海面太阳耀光辐射。为了探究长波红外波段下海面场景的偏振度变化规律，陈兴峰等[20-21]建立了海面场景偏振探测模型，为偏振度信息的获取和利用提供了依据。为研究海上目标在长波红外光谱中的偏振成像特性，Zhang 等[22]利用焦平面长波红外偏振探测器搭建了一套实时偏振成像实验装置，提高了长波红外偏振图像的清晰度。考虑到不同波段下环境因素对偏振探测的影响，胡建明等[23]利用信杂比来表征目标可探测性，具体分析了光照、云层和背景类型与探测性能的关系。海面背景下的空中目标偏振探测性能的影响因素主要包括温度、观测方位角、光源入射角、观测天顶角和探测波段等[24-25]。上述研究工作主要集中在单红外波段偏振探测影响因素分析，存在波段分析单一、偏振特性不明确的问题。

为了提高红外目标探测性能，本文对海面背景下的空中目标红外波段偏振探测链路进行了建模，结合偏振度计算原理，对比了不同波段下目标与海面的偏振度差异，并分析了目标温度、高度和探测俯仰角对提升目标/海面偏振度对比度的作用效果。

收稿日期：2022-11-28；**修回日期**：2023-01-30；**录用日期**：2023-02-24；**网络首发日期**：2023-03-09

基金项目：国家自然科学基金(62105145)、等离子体物理重点实验室基金(6142A04210211)

通信作者：*zhedy@aliyun.com

2　基本原理

2.1　红外辐射模型

探测器接收到的辐射总量包括自发辐射和反射辐射，如图1所示。

总辐射强度$L^{s,p}$可表达为

$$L^{s,p}(\lambda,T,\theta_v,H)=\tau_{atm\text{-}sp}(L^{s,p}_{sfc}+R^{s,p}_{sfc}L_{sun})+L_{atm\text{-}sp},\quad(1)$$

式中：λ表示波长；T表示温度；θ_v表示探测俯仰角；H表示物体距离海平面的高度；上标s表示垂直方向；p表示平行方向；$L^{s,p}_{sfc}$表示物体表面发射辐射；L_{sun}表示太阳辐射；$L_{atm\text{-}sp}$表示传感器与水面之间的大气路径辐射；$R^{s,p}_{sfc}$表示物体表面反射率；$\tau_{atm\text{-}sp}$表示大气透过率。大气透过率$\tau_{atm\text{-}sp}$和大气路径辐射$L_{atm\text{-}sp}$可以利用MODTRAN软件仿真得到。探测器接收的总辐射强度受到波长、探测俯仰角、温度和高度等因素的影响。

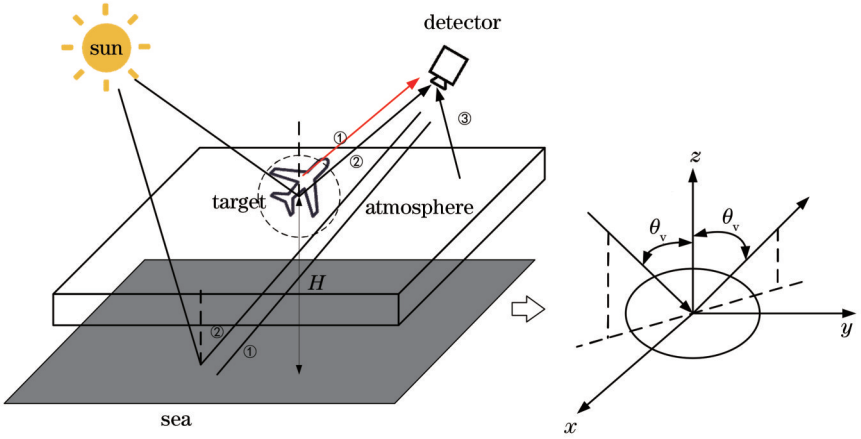

图 1　天基探测系统辐射传输模型图

Fig. 1　Radiation transfer model of space-based detection system

对于物体而言，其发射辐射由物体的发射率和温度决定，即

$$L^{s,p}_{sfc}=\varepsilon^{s,p}_{sfc}(\lambda,\theta_v)L_{bb}(\lambda,T)=\left[1-R^{s,p}_{sfc}(\lambda,\theta_v)\right]L_{bb}(\lambda,T),\quad(2)$$

式中：$\varepsilon^{s,p}_{sfc}$表示物体的发射率；$R^{s,p}_{sfc}$表示物体的反射率；L_{bb}表示黑体辐射。物体的发射辐射是指在绝对温度为T时，黑体的光谱辐射乘以物体的发射率。根据基尔霍夫定律，当不考虑物体透射的能量时，反射率和发射率之和为1。物体的发射率和反射率受到波长和探测俯仰角影响，黑体辐射受到波长和温度的影响。

2.2　偏振探测模型

根据红外辐射模型，探测器接收的垂直和平行分量分别可以表示为

$$\begin{cases}L_s=\tau_{atm\text{-}sp}\left[(1-R^{s}_{sfc})L_{bb}+R^{s}_{sfc}L_{sun}\right]+\dfrac{1}{2}L_{atm\text{-}sp}\\ L_p=\tau_{atm\text{-}sp}\left[(1-R^{p}_{sfc})L_{bb}+R^{p}_{sfc}L_{sun}\right]+\dfrac{1}{2}L_{atm\text{-}sp}\end{cases},\quad(3)$$

式中：L_s和L_p分别表示光波垂直入射面分量和平行入射面分量的辐射强度；R^{s}_{sfc}和R^{p}_{sfc}分别表示光波垂直入射面分量和平行入射面分量的反射率。

在红外探测中，偏振度P可以表示为光波垂直入射面分量和平行入射面分量的辐射强度差值与总辐射强度的比值，相应的表达式为

$$P=\frac{L_s-L_p}{L_s+L_p}。\quad(4)$$

所定义的P未取绝对值，故可通过其正负来判断水平分量和垂直分量的主导性。

海面为透明体，根据Sellmeier公式[26]，折射率为与波长与有关的实数，即

$$n(\lambda)=\sqrt{1+\frac{A\cdot\lambda^2}{\lambda^2-D}+\frac{B\cdot\lambda^2}{\lambda^2-E}+\frac{C\cdot\lambda^2}{\lambda^2-F}},\quad(5)$$

式中，A、B、C、D、E、F为待定常数，不同的物质取值不同。此时海面的R^{s}_{sfc}和R^{p}_{sfc}可以表示为

$$\begin{cases}R^{s}_{sea\text{-}sfc}=\left\{\dfrac{\cos\theta_v-n(\lambda)\cos\left\{\arcsin\left[\sin\theta_v/n(\lambda)\right]\right\}}{\cos\theta_v+n(\lambda)\cos\left\{\arcsin\left[\sin\theta_v/n(\lambda)\right]\right\}}\right\}^2\\ R^{p}_{sea\text{-}sfc}=\left\{\dfrac{n(\lambda)\cos\theta_v-\cos\left\{\arcsin\left[\sin\theta_v/n(\lambda)\right]\right\}}{n(\lambda)\cos\theta_v+\cos\left\{\arcsin\left[\sin\theta_v/n(\lambda)\right]\right\}}\right\}^2\end{cases}。\quad(6)$$

研究目标采用光滑铝表面，为金属等非透明体，其折射率为与波长有关的复数，即

$$N(\lambda)=n_r(\lambda)+\mathrm{j}k(\lambda)=\sqrt{1+\frac{A\cdot\lambda^2}{\lambda^2-D}+\frac{B\cdot\lambda^2}{\lambda^2-E}+\frac{C\cdot\lambda^2}{\lambda^2-F}}+\mathrm{j}\frac{K\rho\lambda}{4\pi},\quad(7)$$

式中：实部$n_r(\lambda)$为通常的折射率；虚部$k(\lambda)$为消光系数，它表示物体对光有吸收；K为物体的吸收系数；ρ为物体的密度。

此时目标的R^{s}_{sfc}和R^{p}_{sfc}可以表示为

$$\begin{cases} R^{s}_{\text{target-sfc}}=\dfrac{\left[n_r(\lambda)-\cos\theta_v\right]^2+n_r^2(\lambda)k^2(\lambda)}{\left[n_r(\lambda)+\cos\theta_v\right]^2+n_r^2(\lambda)k^2(\lambda)} \\ R^{p}_{\text{target-sfc}}=\dfrac{\left[n_r(\lambda)-\dfrac{1}{\cos\theta_v}\right]^2+n_r^2(\lambda)k^2(\lambda)}{\left[n_r(\lambda)+\dfrac{1}{\cos\theta_v}\right]^2+n_r^2(\lambda)k^2(\lambda)} \end{cases}\circ \tag{8}$$

将式(6)和式(8)代入式(4)中可得到理论上偏振的表达式为

$$\begin{cases} P_{\text{sea}}(\lambda,T,\theta_v,H)= \\ \quad\dfrac{(1-w_{\text{sea}})\left(R^{p}_{\text{sea-sfc}}-R^{s}_{\text{sea-sfc}}\right)}{2-(1-w_{\text{sea}})\left(R^{p}_{\text{sea-sfc}}+R^{s}_{\text{sea-sfc}}\right)} \\ P_{\text{target}}(\lambda,T,\theta_v,H)= \\ \quad\dfrac{(1-w_{\text{target}})\left(R^{p}_{\text{target-sfc}}-R^{s}_{\text{target-sfc}}\right)}{2-(1-w_{\text{target}})\left(R^{p}_{\text{target-sfc}}+R^{s}_{\text{target-sfc}}\right)} \end{cases}, \tag{9}$$

式中：$w_{\text{sea}}=L_{\text{sun}}/L_{\text{sea-bb}}$表示太阳辐射和海面的黑体辐射的比值；$w_{\text{target}}=L_{\text{sun}}/L_{\text{target-bb}}$表示太阳辐射和目标的黑体辐射的比值。由式(9)可以发现，理论上偏振度受到波长、温度、入射角和高度等因素影响。目标和海面的偏振度存在差异。s方向和p方向反射率的不同是偏振度差异的重要原因。

在计算得到目标和海面的偏振度后，可以进一步计算目标的偏振度与海面背景的偏振度的差值来衡量和评估天基平台海面背景空中目标的可探测性能，差分偏振度的计算公式为

$$P_{\text{diff}}(\lambda,T,\theta_v,H)=P_{\text{target}}-P_{\text{sea}}\circ \tag{10}$$

分析偏振度方向和大小与探测波长的关系能够有效加强红外偏振技术在天基海面宽波段探测中的应用。利用目标和背景的发射和反射光强计算偏振度，以飞机与海面为例，当太阳高度角取值范围为20°～40°(间隔10°)、探测俯仰角为45°、海面温度为290 K时，0.7～12.0 μm波长范围内的仿真结果如图2所示。

由图2可知：目标偏振度在3.55～12.00 μm波段中受波长影响较大，波动明显，而在0.70～3.55 μm波段之间偏振度波动几乎为0；背景偏振度在0.70～3.55 μm波段内大幅度减小，最后趋于稳定；在0.70～3.55 μm波段内海面偏振度大于目标偏振度，而在3.55～12.00 μm波段内目标偏振度大于海面偏振度。结合目标与背景的红外特性变化特点，考虑大气窗口对于辐射强度的影响，5～8 μm处的大气透过率较低，目标的辐射强度低，不利于探测，因此不选用5～8 μm间的第一个峰值区间作为探测波段。以$\sqrt{2}/2$峰值位置作为探测波段选择标准，选择8.56～10.08 μm为探测波段有利于提高目标与背景的偏振度对比度，增强了天基海面背景空中目标的偏振探测性能。

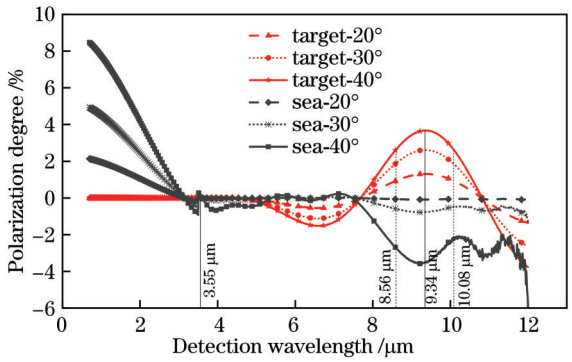

图2　飞机目标与海面背景的宽波段偏振度变化图

Fig. 2　Wide-band polarization degree variation of aircraft target and sea surface background

3　分析与讨论

空中目标在不同飞行高度、表面温度下的红外偏振特性差异较大，且目标和背景的偏振度与探测俯仰角有关。结合红外偏振特性计算模型，在太阳高度角为30°、探测方位角为0°、飞行速度为272.24 m/s时，探究天基海面目标宽波段偏振能力对目标温度、高度和探测俯仰角的敏感度。其中，$R^{s}_{\text{target-sfc}}$、$R^{p}_{\text{target-sfc}}$、$R^{s}_{\text{sea-sfc}}$和$R^{p}_{\text{sea-sfc}}$为随着波长和探测俯仰角变化的值，表1中给出的是波长为0.7μm、探测俯仰角为45°时的示意数值。实验条件如表1所示。

表1　偏振探测性能影响因素的实验参数设置

Table 1　Experimental parameter setting for influencing factors of polarization detection performance

Parameter	Target speed /(m·s^{-1})	Detection azimuth /(°)	Solar altitude angle /(°)	Background category	$R^{s}_{\text{target-sfc}}$	$R^{p}_{\text{target-sfc}}$	$R^{s}_{\text{sea-sfc}}$	$R^{p}_{\text{sea-sfc}}$
Description	272.24	0	30	Sea	0.926	0.858	0.053	0.003

3.1　目标温度的影响

以280～300 K为实验目标温度T的取值范围，在0.7～12.0 μm波段内，探究红外辐射相当条件下偏振探测性能与温度的关系，结果如图3所示。

由图3可知：温度越高，目标偏振度越大；在4.85～7.65 μm波段内，水平偏振占主导，偏振度先增大后减小；在7.65～10.82 μm波段内，垂直偏振占主导，偏振度先增大至峰值，后逐渐减小。计算目标/背景差分偏振度与温度的关系，结果如图4所示。

由图4可知，目标与海面的温差越大，目标/海面差分偏振度越大。不同波段内目标/海面差分偏振度对温度的敏感度不同：差分偏振度在0.7～4.0 μm波段内多为负值，在4.88～10.78 μm波段内波动较大，在9.33 μm附近取到峰值，且在峰值附近对温度的敏

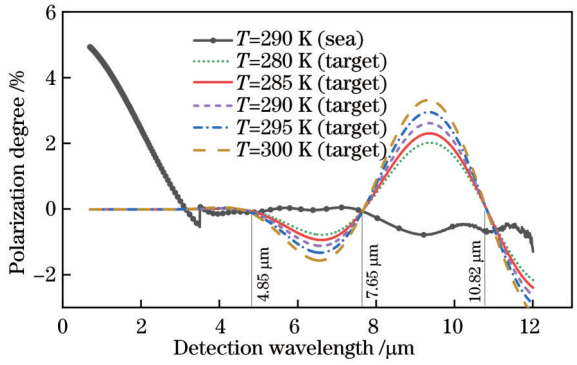

图 3　宽波段目标和海面的偏振度与目标温度的关系图

Fig. 3　Wide-band polarization degree of target and sea surface varying with target temperature

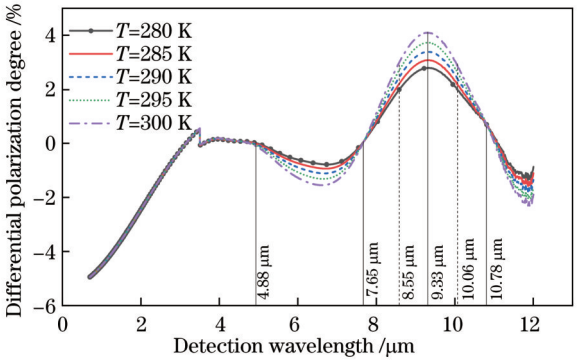

图 4　宽波段目标/海面差分偏振度与目标温度的关系图

Fig. 4　Wide-band differential polarization degree of target and sea surface varying with target temperature

感度显著增强。因此，考虑到目标不同温度影响的情况下，以 $\sqrt{2}/2$ 峰值位置作为探测波段选择标准应该选择 8.55～10.06 μm 波段进行探测。

3.2　目标高度的影响

目标高度不同引起的辐射强度差异会影响偏振探测性能。以 3～12 km 为高度 H 的取值范围（间隔 3 km），在 0.7～12.0 μm 波段内计算飞机在不同高度下的偏振度，结果如图 5 所示。

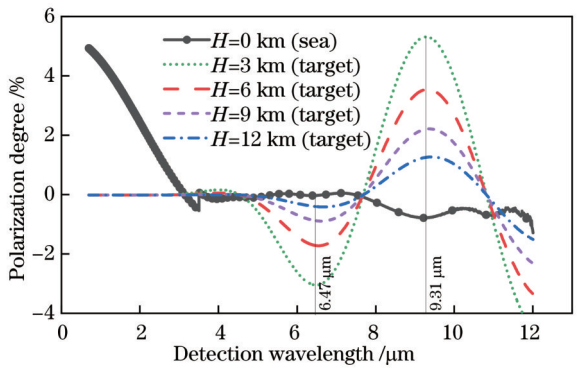

图 5　宽波段目标和海面偏振度与目标高度的关系图

Fig. 5　Wide-band polarization degree of target and sea surface varying with target height

由图 5 可知：目标飞行高度越高，偏振度越小；在短波红外波段中，背景偏振度大于目标偏振度；在中波与长波红外波段中，目标偏振度大于背景偏振度，且目标偏振度在 6.47 μm 和 9.31 μm 处取到偏振度极大值。对比图 4 可知，高度比温度对目标偏振度的影响更大，不同高度下目标偏振度变化差值最高可达到 4%。利用差分偏振度分析目标与背景的偏振度差值在不同波段与目标高度的关系，如图 6 所示。

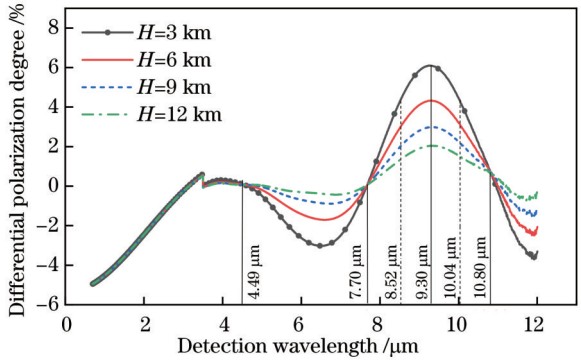

图 6　宽波段目标/海面差分偏振度与目标高度的关系图

Fig. 6　Wide-band differential polarization degree of target and sea surface varying with target height

由图 6 可知，不同波段内目标/海面差分偏振度对高度的敏感度不同：目标/海面差分偏振度在 0.7～4.0 μm 波段内与高度基本无关；随着波长的增加，差分偏振度迅速降低；在近红外波段中，改变飞行高度对于偏振探测没有增益；在 4.49～10.80 μm 波段内，目标/海面差分偏振度对高度的敏感度较高，且存在峰值特性。因此，综合考虑目标的偏振度大小与大气窗口对于辐射强度的影响，8.52～10.04 μm 窄带光谱在不同探测高度下均有优异的偏振探测能力。

3.3　探测俯仰角的影响

探测角度变化会导致物体表面反射率改变，从而影响偏振度结果。以 0～90°为探测俯仰角 θ_v 的取值范围（间隔为 15°），在 0.7～12.0 μm 波段内，计算目标和背景在不同探测俯仰角下各波段的偏振度，结果如图 7 所示。

由图 7 可知，当探测俯仰角减小时，虽然天基探测平台距离上更加接近目标与海面，但是目标和海面的偏振度降低了。在 0.70～7.65 μm 波段内水平偏振占主导，偏振度先减小后增大再减小。在 7.65～10.81 μm 波段内，垂直偏振占主导，偏振度先增加至峰值后逐渐减小。为了更加清晰地分析目标和背景的偏振特性差异，计算了不同波段下差分偏振度与探测俯仰角的关系，结果如图 8 所示。

由图 8 可知，不同波段内目标/背景差分偏振度对探测俯仰角的敏感度不同：在 0.70～3.13 μm 波段内目标/背景差分偏振度对探测俯仰角的敏感度高，且随着波长的增加而降低，故在该波段内增大探测俯仰角

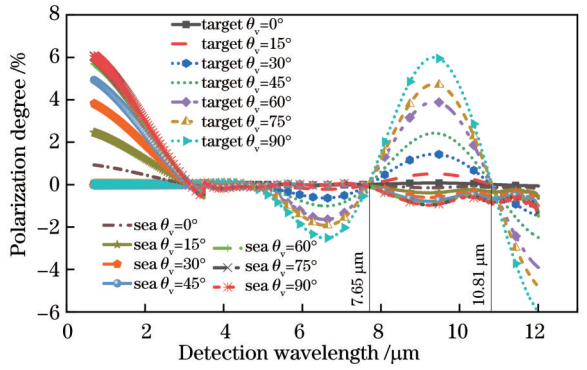

图 7　宽波段目标和海面偏振度与探测俯仰角的关系图

Fig. 7　Wide-band polarization degree of target and sea surface varying with detection pitch angle

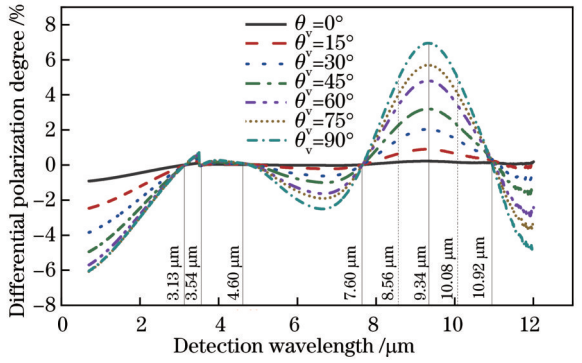

图 8　宽波段目标/海面差分偏振度与探测俯仰角的关系图

Fig. 8　Wide-band differential polarization degree of target and sea surface varying with detection pitch angle

度会增强探测能力；在 3.54～4.60 μm 波段内差分偏振度较小，并且几乎没有变化，故不适合探测；在 4.60～10.92 μm 波段内差分偏振度对探测俯仰角度的敏感度较高，且存在峰值特性。在峰值位置处，探测俯仰角、目标温度和目标高度等因素对偏振度的影响达到最佳平衡，偏振度达到最大，有利于探测。以 $\sqrt{2}/2$ 峰值位置作为探测波段选择标准，在 8.56～10.08 μm 窄带波段内，增加探测俯仰角可使得探测器接近掠地状态，有利于提高偏振探测效果。在实际探测中，还应综合考虑大气路径、太阳方位角等因素，从而保证在 8.56～10.08 μm 窄带波段内选择合适的大角度以达到良好的探测效果。

4　结　　论

针对海面空中目标红外偏振探测存在最佳探测波段不明的问题，理论验证并分析了波长对偏振度的影响，开展了宽波段天基海面偏振探测成像仿真实验，并结合偏振度计算方法探究了目标温度、目标高度和探测俯仰角对目标和背景偏振特性的影响规律。基于目标和背景的红外偏振特性在各波段内的显著变化规律，可以确定最佳探测波段为 8.56～10.08 μm，且垂直偏振分量占主导。在最佳探测波段内，当增大空中目标与海面的温差、降低目标的飞行高度和选择探测俯仰角为较大角度时，天基海面空中目标偏振探测的能力可得到提高。本文结果为研究海面空中目标的红外偏振辐射特性的几何敏感性和促进多波段目标隐身与识别技术的发展提供了有益的参考。

参　考　文　献

[1] Cremer F, Schwering P B W, de Jong W, et al. Infrared polarization measurements of targets and backgrounds in a marine environment[J]. Proceedings of SPIE, 2001, 4370: 169-180.

[2] Zhang J H, Zhang Y, Shi Z G. Enhancement of dim targets in a sea background based on long-wave infrared polarisation features [J]. IET Image Processing, 2018, 12(11): 2042-2050.

[3] 倪歆玥, 余书田, 唐玉俊, 等. 海雾中舰船目标的偏振探测能力研究[J]. 红外与毫米波学报, 2021, 40(1): 96-101.
Ni X Y, Yu S T, Tang Y J, et al. The research on polarimetric detection capability of ship targets in the sea fog[J]. Journal of Infrared and Millimeter Waves, 2021, 40(1): 96-101.

[4] 宫剑, 吕俊伟, 刘亮, 等. 红外偏振图像的舰船目标检测[J]. 光谱学与光谱分析, 2020, 40(2): 586-594.
Gong J, Lü J W, Liu L, et al. Ship target detection based on infrared polarization image[J]. Spectroscopy and Spectral Analysis, 2020, 40(2): 586-594.

[5] He C, Chang J T, Salter P S, et al. Revealing complex optical phenomena through vectorial metrics[J]. Advanced Photonics, 2022, 4(2): 026001.

[6] Liu F, Zhang S C, Han P L, et al. Depolarization index from Mueller matrix descatters imaging in turbid water[J]. Chinese Optics Letters, 2022, 20(2): 022601.

[7] Bijl P, Hogervorst M A. Test method for multiband imaging sensors[J]. Proceedings of SPIE, 2003, 5076: 208-219.

[8] Lang J W, Wang Y M, Xiao X Z, et al. Study on shortwave infrared long-distance imaging performance based on multiband imaging experiments[J]. Optical Engineering, 2013, 52(4): 045008.

[9] Huang Y, Zhang J J, Zhou J H, et al. Polarization-robust mid-infrared carpet cloak with minimized lateral shift[J]. Photonics Research, 2021, 9(6): 944-949.

[10] Tong J C, Luo H, Suo F, et al. Epitaxial indium antimonide for multiband photodetection from IR to millimeter/terahertz wave [J]. Photonics Research, 2022, 10(5): 1194-1201.

[11] Yu K, Zhang W, Qian M D, et al. Multiband metamaterial emitters for infrared and laser compatible stealth with thermal management based on dissipative dielectrics[J]. Photonics Research, 2023, 11(2): 290-298.

[12] Yuan H, Wang X R, Yuan Y, et al. Space-based full chain multi-spectral imaging features accurate prediction and analysis for aircraft plume under sea/cloud background[J]. Optics Express, 2019, 27(18): 26027-26043.

[13] 袁航, 王晓蕊, 袁影, 等. 天基平台海云背景下飞机全链路成像特征建模及分析[J]. 红外与激光工程, 2020, 49(2): 0204004.
Yuan H, Wang X R, Yuan Y, et al. Modeling and analysis of aircraft full-chain imaging characteristics in the sea surface and clouds from a space-based platform[J]. Infrared and Laser Engineering, 2020, 49(2): 0204004.

[14] Ni X Y, Yu S T, Su X F, et al. Detection spectrum optimization of stealth aircraft targets from a space-based infrared platform[J]. Optical and Quantum Electronics, 2022, 54(3): 151.

[15] Zhou X X, Ni X Y, Zhang J W, et al. A novel detection performance modular evaluation metric of space-based infrared system[J]. Optical and Quantum Electronics, 2022, 54(5): 274.

[16] 史浩东, 王稼禹, 李英超, 等. 复杂海况下海洋生态环境多维

度光学监测方法[J]. 光学学报, 2022, 42(6): 0600004.
Shi H D, Wang J Y, Li Y C, et al. Multi-dimensional optical monitoring method of marine ecological environment under complex sea conditions[J]. Acta Optica Sinica, 2022, 42(6): 0600004.
[17] 王启超, 赵大鹏, 汪家春, 等. 多光谱偏振探测对伪装目标的识别研究[J]. 光电工程, 2013, 40(3): 29-34.
Wang Q C, Zhao D P, Wang J C, et al. Recognition of camouflage targets with multi-spectral polarization detection system[J]. Opto-Electronic Engineering, 2013, 40(3): 29-34.
[18] 王霄, 高思莉, 金璐, 等. 空中目标多波段红外辐射特性描述与仿真分析[J]. 光子学报, 2020, 49(5): 0511002.
Wang X, Gao S L, Jin L, et al. Multi-band infrared radiation characterization and simulation analysis for aerial target[J]. Acta Photonica Sinica, 2020, 49(5): 0511002.
[19] 李岩松, 赵慧洁, 李娜, 等. 基于中红外偏振的海面太阳耀光背景下的目标探测[J]. 中国激光, 2022, 49(19): 1910004.
Li Y S, Zhao H J, Li N, et al. Detection of marine targets covered in sun glint based on mid-infrared polarization[J]. Chinese Journal of Lasers, 2022, 49(19): 1910004.
[20] 陈兴峰, 顾行发, 程天海, 等. 真实海洋表面的太阳耀光偏振辐射特性仿真与分析[J]. 光谱学与光谱分析, 2011, 31(6): 1648-1653.
Chen X F, Gu X F, Cheng T H, et al. Simulation and analysis of polarization characteristics for real sea surface sunglint[J]. Spectroscopy and Spectral Analysis, 2011, 31(6): 1648-1653.
[21] 张景华, 张焱, 石志广. 基于长波红外的海面场景偏振特性分析与建模[J]. 红外与毫米波学报, 2018, 37(5): 586-594.
Zhang J H, Zhang Y, Shi Z G. Study and modeling of infrared polarization characteristics based on sea scene in long wave band [J]. Journal of Infrared and Millimeter Waves, 2018, 37(5): 586-594.
[22] Zhang X M, Zhang Y, Zhao H, et al. Research on long wave infrared imaging of sea target[J]. Proceedings of SPIE, 2022, 12169: 121690A.
[23] 胡建明, 乔凯, 智喜洋, 等. 天基观测条件下复杂环境对空中弱小目标可探测性的影响[J]. 红外与毫米波学报, 2019, 38(3): 351-357.
Hu J M, Qiao K, Zhi X Y, et al. Influence of complex environment on the detectability of weak and small aerial target under space-based observation mode[J]. Journal of Infrared and Millimeter Waves, 2019, 38(3): 351-357.
[24] 申慧彦, 周浦城, 王峰. 水面溢油污染的多角度多波段偏振特性研究[J]. 海洋环境科学, 2012, 31(2): 241-245, 249.
Shen H Y, Zhou P C, Wang F. Multi-angle and multi-band polarimetric characteristic of spilled oil pollution on water surface [J]. Marine Environmental Science, 2012, 31(2): 241-245, 249.
[25] 李雅男, 孙晓兵, 毛永娜, 等. 空间目标光谱偏振特性[J]. 红外与激光工程, 2012, 41(1): 205-210.
Li Y N, Sun X B, Mao Y N, et al. Spectral polarization characteristic of space target[J]. Infrared and Laser Engineering, 2012, 41(1): 205-210.
[26] 凌晋江, 李钢, 张仁斌, 等. 偏振光谱BRDF建模与仿真[J]. 光谱学与光谱分析, 2016, 36(1): 42-46.
Ling J J, Li G, Zhang R B, et al. Modeling and simulation of spectral polarimetric BRDF[J]. Spectroscopy and Spectral Analysis, 2016, 36(1): 42-46.

Simulation and Analysis of Infrared Polarization Radiation Characteristics of Air Targets Against Sea Surface

Zhu Deyan[1,2*], Fu Xiaoxuan[1,2], Tang Junwei[1,2], Liu Xiaolei[3]

[1]*College of Astronautics, Nanjing University of Aeronautics and Astronautics, Nanjing* 210001, *Jiangsu, China*;
[2]*Key Laboratory of Space Photoelectric Detection and Sensing of Industry and Information Technology, Nanjing University of Aeronautics and Astronautics, Nanjing* 210001, *Jiangsu, China*;
[3]*Remote Sensing Satellite General Department of China Academy of Space Technology, Beijing* 100098, *China*

Abstract

Objective The development of space-based air target detection against sea surface is conducive to improving the country's ocean sensing capability and providing an effective way for the refined detection and identification of distant sea targets. The traditional infrared detection method is greatly affected by environmental factors and is prone to problems such as target submersion in the background. In the case of low contrast between target and background infrared radiation intensity, the combination of polarization characteristic difference with infrared intensity detection can significantly improve the detection and identification capability of the system. With the continuous development of infrared multi-band imaging and guidance technology, how to use the polarization characteristics and select the band to be used to improve the target detection capability has become a difficult issue in space-based air target detection against sea background. In order to improve the infrared target detection performance, in this study, we model the infrared band polarization detection link of airborne targets in the sea surface background, combine the polarization calculation principle, compare the difference of polarization between target and sea surface in different bands, and analyze the effect of target temperature, height, and detection pitch angle on improving the contrast of target/sea surface polarization. The research results can be helpful to improve the infrared polarization detection capability of space-based sea surface air targets.

Methods In this study, simulations are performed to compare and analyze the target and background in the band of 0.7-12.0 μm in combination with polarization. Firstly, the radiation transmission link of the space/sea-based airborne target

detection system is established by combining the reflection model and spontaneous radiation model, and the relevant environmental parameters are obtained by using MODTRAN software simulation. Then, the Sellmeier formula is combined with the reflectivity calculation method to calculate the polarization of the target and the sea surface and explore the relationship among the polarization and wavelength, temperature, detection pitch angle, and height. The difference between the polarization of the target and the sea surface is further calculated to evaluate the detectability performance of the air targets against sea surface. The optimal detection band is clarified by simulation experiments on aircraft target and sea surface. Finally, based on the calculation model of the infrared polarization characteristics, the sensitivity of the wide-band polarization degree of the target and the sea surface to the target temperature, height, and detection pitch angle is explored at a solar altitude angle of 30°, a detection azimuth angle of 0°, and a flight speed of 272.24 m/s. The relationship among the vertical polarization component, the horizontal polarization component, and wavelength is analyzed by combining the variation law of polarization of the target and the sea surface. In addition, the parameter settings to improve the detection performance at the best wavelength are clarified by considering the atmospheric path, solar azimuth, and other factors.

Results and Discussions According to the infrared characteristics of the target and the background change, it is found that there are two peak intervals of differential polarization between the target and the sea surface. By considering the influence of the atmospheric window on the radiation intensity, the atmospheric transmittance at 5-8 μm is low, which is not conducive to detection. By using the $\sqrt{2}/2$ peak position as the detection band selection criteria, the detection band of 8.56-10.08 μm is conducive to improving the contrast between the polarization of the target and the background and enhancing the polarization detection performance (Fig. 2). The effects of the target temperature, target height, and detection pitch angle on the detection performance are explored in different wavebands. Firstly, as the temperature difference between the target and the sea surface gets larger, the target/sea surface differential polarization degree becomes greater. In addition, the sensitivity of target/sea surface differential polarization degree to temperature is different in different wavelength bands (Fig. 4). Secondly, as the target height gets higher, the polarization gets smaller (Fig. 5). The sensitivity of target/sea surface differential polarization degree to target height varies in different wavelength bands (Fig. 6). Thirdly, the polarization degree of the target and the sea surface decreases when the detection pitch angle decreases, although the space-based detection platform is closer to the target and the sea surface in terms of distance (Fig. 7). The detection pitch angle increases in the narrow band of 8.56-10.08 μm, which makes the detector close to the ground-skimming state and is conducive to improving the polarization detection effect. In the actual detection, the atmospheric path, solar azimuth, and other factors should also be taken into account to ensure that the selection of the appropriate large angle in the narrow band of 8.56-10.08 μm can achieve good detection results (Fig. 8).

Conclusions For the problem that the best detection band of air target infrared polarization detection against sea surface is unknown, the influence of wavelength on polarization degree is theoretically verified and analyzed, and the simulation experiment of wide-band space-based polarization detection imaging against sea surface is carried out. The influence law of target temperature, target height, and detection pitch angle on target and background polarization characteristics is explored in combination with the polarization degree calculation method. On the basis of the significant variation of the infrared polarization characteristics of the target and the background in each band, the best detection band can be determined to be 8.56-10.08 μm, and the vertical polarization component dominates. In the best detection band, increasing the temperature difference between the air target and the sea surface, reducing the flight height of the target, and selecting a larger angle of detection pitch are conducive to enhancing the polarization detection capability of space-based air targets against sea surface. This study provides a useful reference for studying the geometric sensitivity of infrared polarization radiation characteristics of air targets against sea surface and promoting the development of multi-band target stealth and identification technology.

Key words measurement; polarization imaging; infrared characteristics; sea background; space-based detection; degree of polarization